Shock Polars for Dissociating Gases

GEORGE R. INGER* AND DONALD A. MEIS†
Douglas Aircraft Company Inc., Santa Monica, Calif.

The hodograph or polar diagram for oblique shock waves is generalized to the case of dissociating diatomic gases, assuming either a chemically frozen flow or complete thermochemical equilibrium behind the shock. A dissociated ambient gas condition is treated also. Several examples of the shock-polar diagram with dissociation are constructed for hypersonic shock Mach numbers. It is shown that in the presence of equilibrium dissociation the detachment point can occur at a slightly supersonic post-shock velocity, in contrast to the subsonic condition prevailing in perfect gas flow. It is shown also that large degrees ($\geq$25%) of ambient dissociation yield post-shock dissociation levels that are considerably less than the preshock value over a significant portion of the shock polar.

Nomenclature

a = speed of sound
h_D = dissociation energy
h = specific enthalpy
M = Mach number
p = static pressure
R_M = molecular gas constant
T = temperature
U = streamwise velocity component
V = normal velocity component
α = atom mass fraction
β = enthalpy coefficient
γ = specific heat ratio
$\hat{\gamma}$ = effective specific heat ratio [Eq. (19)]
$\bar{\gamma}$ = frozen specific heat ratio
θ = flow angle
μ = Mach angle
ρ = density
σ = shock angle

Subscripts

1 = freestream condition
2 = condition behind the shock
e = denotes equilibrium
M = denotes molecule
S = sonic
T = detachment

Introduction

SEVERAL problem areas of current importance in gasdynamics involve shock waves that either occur in or generate a significantly dissociated gas flow. Consequently, the study of high-temperature real gas effects on the flow properties behind oblique shock waves is of considerable interest. One of the tools that has been used for study in conventional, perfect gasdynamics is the shock-polar diagram.[1, 2] Although this diagram can be used for quantitative analysis and occasionally has been so employed, it primarily serves to complement perfect gas flow tables (such as those in Ref. 3) by providing a graphical display of the velocity vectors and wave geometry for all of the possible oblique shock wave solutions pertaining to a given freestream condition. A generalization of the polar diagram to the case of dissociating gas flows, therefore, would be of interest as a complement to existing real gas shock tables, such as those of Feldman[4] and of Ref. 5 for air.

Accordingly, such a generalization is given in this paper for the limiting conditions of either equilibrium or completely frozen post-shock flow. As is well known, the former situation occurs when the ambient density is high enough and the shock velocity is low enough that the post-shock relaxation time for dissociation and vibrational excitation is negligibly short compared to the flow time. On the other hand, completely frozen flow results under the conditions of very low ambient density and high velocity, where the relaxation time is so long compared to the flow time that the chemical and vibrational states, well downstream of the shock, are the same as those in the freestream. In intermediate flow regimes where a finite post-shock relaxation exists, the details of the nonequilibrium process must be taken into account in analyzing the gas properties near the shock. However, the foremention limiting states are still of interest in that they can be associated with a given set of freestream conditions as upper and lower bounds on the properties of the shocked gas.

The basic hodograph relations are derived in this paper for the case of a dissociated and/or vibrationally excited diatomic gas, including the possible presence of a dissociated freestream. A diatomic gas model is employed because it describes a number of gases (e.g., pure oxygen, nitrogen, and the halogens) that are in themselves of experimental importance, and because it is known also to be representative of a dissociated air mixture as well. Moreover, the relative simplicity of the model affords useful analytical insight into the basic real gas effects involved in flow problems. Following a discussion of the hodograph relations, an analysis of the effects of dissociation on the relative location of the sonic and detachment points on the hodograph is given. Finally, several example shock polars for hypersonic flow in both perfect and dissociated ambient gas are presented and discussed.

Hodograph Relations for Dissociating Diatomic Gas

Consider the steady, adiabatic flow of a dissociating diatomic gas across an oblique shock discontinuity (Fig. 1). In terms of the velocity components U and V, parallel and normal, respectively, to the velocity U_1 of the incoming undisturbed freestream, the following equations govern the change in state across the wave[6]:

$$\rho_1 U_1 = \rho_2(U_2 - V_2 \cot\sigma) \quad (1)$$

$$\tan\sigma = (U_1 - U_2/V_2) \quad (2)$$

$$p_2 + \rho_2(U_2 \sin\sigma - V_2 \cos\sigma)^2 = p_1 + \rho_1 U_1^2 \sin^2\sigma \quad (3)$$

Received by IAS October 22, 1962; revision received May 20, 1963. The authors wish to thank W. G. Vincenti and C. T. Hsu for their stimulating comments and criticisms on the manuscript, and N. Rott and R. J. Hakkinen for their helpful discussions on this work.

* Formerly Gasdynamics Research Specialist, Missile Aerodynamics Section, Missile and Space Systems Division; presently Member of the Technical Staff, Aerodynamics and Propulsion Laboratories, Aerospace Corporation. Member AIAA.

† Aerodynamicist, Advance Missile Technology, Missile and Space Systems Division.

$$p = R_M(1 + \alpha)\rho T \tag{4}$$

$$\beta_1 \frac{p_1}{\rho_1} + \frac{U_1^2}{2} + \alpha_1 h_D = \beta_2 \frac{p_2}{\rho_2} + \frac{U_2^2 + V_2^2}{2} + \alpha_2 h_D = h_T \tag{5}$$

where the subscripts 1 and 2 indicate conditions ahead of and behind the shock, and ρ, T, α, R_M, and h_D are the density, temperature, atom mass fraction, undissociated gas constant, and dissociation energy, respectively. The parameter β is a nondimensional enthalpy coefficient of the dissociated gas mixture defined by

$$\beta = \frac{\rho h}{p} = \left(\frac{1 - \alpha}{1 + \alpha}\right)\beta_M + \frac{5\alpha}{1 + \alpha} \tag{6}$$

where h is the temperature-sensible enthalpy, and

$$\beta_M \equiv T^{-1}\int_0^T \left(\frac{Cp_M}{R_M}\right) dT$$

is an averaged nondimensional molecular specific heat that lies between $\frac{7}{2}$ (no vibration) and $\frac{9}{2}$ (completely excited vibration). To simplify the analysis and, at the same time, preserve the essential qualitative features pertinent to molecular vibration, β_M is assumed to be an arbitrary constant. (This is a reasonable approximation when changes in vibrational energy are small compared to the energy in dissociation.) A plot of β vs α for several values of β_M is shown in Fig. 2.

The formulation of the basic relations is completed by the addition of an equation that determines the degree of dissociation α_2 behind the shock. Here, attention is confined to the two limiting cases of thermochemical behavior in the shocked gas: 1) chemically and vibrationally frozen flow, or 2) complete equilibrium attained behind the shock. In case 1, the simple solutions are $\alpha_2 = \alpha_1$ and $\beta_2 = \beta_1$. However, when case 2 applies, α_2, which is a function of p_2 and T_2, may be approximated by the relation[7, 8]

$$\frac{\alpha_{2e}^2}{1 - \alpha_{2e}^2} \simeq \frac{p_0}{4p_2}\exp\left(C - \frac{T_D}{T_2}\right) = \frac{p_D}{p_2}\exp\left(-\frac{T_D}{T_2}\right) \tag{7}$$

where C is a constant, p_0 is the atmospheric pressure, $p_D = p_0 e^c/4$ is a characteristic dissociation pressure, and $T_D = h_D/R_M$ is the dissociation temperature. It should be noted that any preshock dissociation α_1 that may be present is assumed uniform but not necessarily in equilibrium with p_1 and T_1. In fact, in many practical applications, the presence of a dissociated freestream is the result of a highly nonequilibrium flow history upstream of the shock front.[9, 10]

A relationship between V_2 and U_2 now can be derived readily from Eqs. (1–5) as follows. First, Eq. (2) is substituted into Eqs. (1) and (3) to yield

$$\frac{\rho_2}{\rho_1} = \frac{U_1(U_1 - U_2)}{U_1U_2 - (U_2^2 + V_2^2)} \tag{8}$$

and

$$\frac{p_2}{p_1} = 1 + \frac{\rho_1 U_1}{p_1}(U_1 - U_2) \tag{9}$$

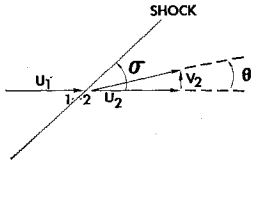

Fig. 1 Flow configuration.

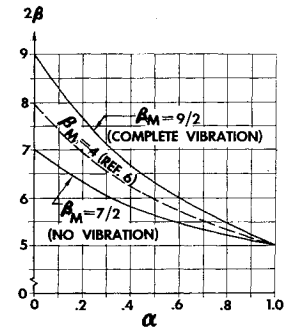

Fig. 2 Enthalpy parameter β.

Next, Eq. (4) is used in Eq. (5) to obtain

$$\frac{T_2}{T_1} = \frac{\beta_1(1 + \alpha_1)}{\beta_2(1 + \alpha_2)} + \frac{U_1 - (U_2^2 + V_2^2)}{2\beta_2 R_M(1 + \alpha_2)T_1} - \frac{(\alpha_2 - \alpha_1)h_D}{\beta_2 R_M(1 + \alpha_2)T_1} \tag{10}$$

Then, by substituting Eqs. (8–10) into (4), the desired hodograph relation is arrived at after considerable algebraic manipulation. Now the nondimensional variables are introduced:

$$\eta = \frac{V_2}{V^*} \qquad \xi = \frac{U_2}{V^*} \qquad \xi_1 = \frac{U_1}{V^*} \qquad H_D = \frac{2h_D}{U_1^2}$$

$$\epsilon = \frac{2\beta_1 R_M T_1(1 + \alpha_1)}{U_1^2} = \frac{2\beta_1}{\bar{\gamma}_1 M_1^2} \tag{11}$$

$$\lambda = \frac{2(\beta_2 - \beta_1)}{2\beta_1 - 1} = \frac{2\bar{\gamma}_1}{\bar{\gamma}_1 + 1}\left(\frac{\beta_2}{\beta_1} - 1\right)$$

where

$$V^* \equiv [2(h_T - \alpha_1 h_D)/(2\beta_1 - 1)]^{1/2} = [(1 + \epsilon)/(2\beta_1 - 1)]^{1/2}U_1$$

is the speed of sound at sonic velocity (as defined in conventional gasdynamics) when based on the total enthalpy exclusive of the ambient dissociation energy, and M_1 is the "frozen" freestream Mach number based on the specific heat ratio $\bar{\gamma}_1 = \beta_1/(\beta_1 - 1)$. The resulting relation can be expressed as follows:

$$\left(\frac{\eta}{\xi_1 - \xi}\right)^2 = \frac{(1 + \lambda)\xi_1\xi - 1 + [(2\beta_1 - 1)\epsilon\lambda\xi/2\beta_1(1 + \epsilon)(\xi_1 - \xi)] + [\xi_1(\alpha_2 - \alpha_1)H_D/(1 + \epsilon)(\xi_1 - \xi)]}{\{[2/(\bar{\gamma}_1 + 1)] + \lambda\}\xi_1^2 - (1 + \lambda)\xi_1\xi + 1 + [\epsilon\lambda(2\beta_1 - 1)/2\beta_1(1 + \epsilon)]} \tag{12}$$

For each set of freestream conditions, Eq. (12) describes all possible velocity vectors behind an oblique compression wave with α_2 and β_{M2} as parameters and is, thus, the desired generalization of the classical hodograph relationship for a perfect gas [to which Eq. (12) reduces by setting $\alpha_1 = \alpha_2 = 0$ and $\beta_1 = \beta_2 = \frac{7}{2}$]. In the case of a frozen shock transition, Eq. (12), as expected, simplifies to the hodograph equation pertaining to a perfect gas of specific heat ratio $\bar{\gamma}_1(\alpha_1)$. On the other hand, when equilibrium prevails behind the shock, Eq. (12) must be complemented by a second hodograph relation that represents the locus of points satisfying the equilibrium composition Eq. (7). Substituting Eqs. (8–11) into Eq. (7) and solving for $\eta(\xi)$ with α_2, β_{M2} as parameters, one finds this second "composition locus" to be

$$\eta^2 = \frac{\beta_2(2\beta_1 - 1)(1 + \alpha_{2e})H_D}{(1 + \epsilon)\ln\{[\alpha_2^2/(1 - \alpha_{2e}^2)](p_1/p_D)[1 + (1 + \epsilon)\bar{\gamma}_1 M_1^2\xi_1(\xi_1 - \xi)/(2\beta_1 - 1)]\}} + \xi_1^2 - \xi^2 + \frac{(2\beta_1 - 1)\epsilon}{1 + \epsilon} - \frac{(2\beta_1 - 1)(\alpha_{2e} - \alpha_1)H_D}{1 + \epsilon} \tag{13}$$

Thus, the true equilibrium shock-polar curve is given by a simultaneous solution to Eqs. (12) and (13). Graphically, this result is obtained easily, as illustrated in Fig. 3.‡ In connection with such constructions, it is noted that, for a

‡ The specific values of the parameters used in calculating this example and the other cases to follow are given in Table 1.

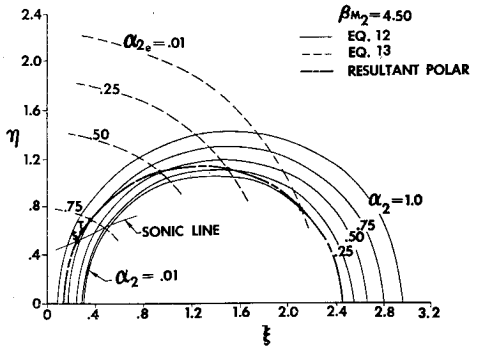

Fig. 3 Construction of shock polar for equilibrium-dissociated flow; case 1, $\alpha_1 = 0$.

given value of ξ_1, the parameter ϵ enters the foregoing hodograph relations only when $\alpha_2 \neq \alpha_1$ or $\lambda \neq 0$. Now a significant amount of post-shock dissociation or vibrational excitation relative to the ambient gas occurs when the Mach number of the undisturbed gas stream is high (in which case ϵ is negligible, since $\epsilon \leqslant 0.05$ for $M_1 \geqslant 8$); therefore, ϵ can be neglected for all values of M_1 in many cases of practical interest.

By means of the relations

$$\tan\theta = V_2/U_2 = \eta/\xi$$
$$\tan\sigma = (U_1 - U_2)/V_2 = (\xi_1 - \xi)/\eta \qquad (14)$$

the wave angle and the flow-deflection angle are determined from the polar diagram as indicated in Fig. 4. In the usual way, one also identifies points on the shock polar which lie to the right and left of the tangent point T (maximum flow deflection) as solutions pertaining to weak and strong shock waves, respectively (e.g., points P and Q). The two limiting cases that correspond to $\theta = 0$ are as follows:

Mach Wave

$$\xi = \xi_1 > 1 \qquad \sigma = \arcsin(M_1^{-1}) \qquad (15)$$

Normal Shock Wave

$$\xi = \xi_N < 1 \qquad \sigma = \pi/2 \qquad (16)$$

These intercepts are given by the two roots of Eq. (12) for $\eta = 0$:

$$2(\xi)_{\eta=0} = \frac{(1+\lambda)\xi_1^2 + 1 + K\epsilon}{(1+\lambda)\xi_1} \pm \frac{\{[(1+\lambda)\xi_1^2 - 1 - K\epsilon]^2 + 4(1+\lambda)\xi_1^2\,[K\epsilon + (\alpha_2 - \alpha_1)H_D/(1+\epsilon)]\}^{1/2}}{(1+\lambda)\xi_1} \qquad (17)$$

where $K \equiv (2\beta_1 - 1)\lambda/2\beta_1(1+\epsilon)$. The positive root yields $\xi = \xi_1$, since the conditions $\alpha_2 = \alpha_1$ and $\lambda = 0$ are physically meaningful only for a Mach wave. The negative radical yields the normal shock solution ξ_N as a function of α_2 and λ. It is seen that the resulting value of ξ_N is a positive, real number, provided

$$\frac{(\alpha_2 - \alpha_1)H_D}{1+\epsilon} \geq -\left\{K\epsilon + \frac{(1+\lambda)\xi_1^2}{4} \times \left[1 - \frac{1+K\epsilon}{(1+\lambda)\xi_1^2}\right]^2\right\} \qquad (18)$$

a condition that always is satisfied when $\alpha_2 = \alpha_1$. In cer-

Table 1 Values of parameters used in numerical examples

Case	U_1, fps	Oxygen, $p_D = 6.25 \times 10^8$ psf: M_1 for $\alpha_1 = 0$	ρ_1, slugs/ft^3	T_1, °R	β_{M1}
1	20,000	17.2	7.3×10^{-7}	628	3.5
2	15,000	13.4	3.3×10^{-6}	580	3.5
3	10,000	10.85	3.5×10^{-5}	392	3.5

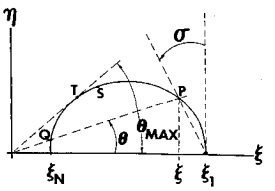

Fig. 4 Geomtery of shock-polar diagram.

tain cases where $\alpha_1 > 0$, depending on ξ_1, ϵ, and λ, Eq. (18) also admits solutions for $\alpha_2 < \alpha_1$, as will be shown below.

Location of the Sonic and Detachment Points

Having established the generalized shock-polar relations for a dissociating diatomic gas, one can derive now the corresponding relations for the locus of points with sonic post-shock velocity and the location of the detachment point where $\theta = \theta_{\max}$. Consider first the sonic condition. Here, one can write

$$U_2^2 + V_2^2 = a_2^2 = \hat{\gamma}_2 R_M (1 + \alpha_2) T_2 \qquad (19)$$

where a_2 is the speed of sound behind the shock, and $\hat{\gamma}_2$ is a specific heat ratio appropriate to the definition of a_2 in either a frozen- or equilibrium-dissociated gas. For frozen flow, $\hat{\gamma}_2 = \bar{\gamma}_2 = \beta_2/(\beta_2 - 1)$, whereas in an equilibrium gas,

$$\hat{\gamma}_{2e} = \frac{\gamma_{2e}}{\{1 - [p_2/(1+\alpha_{2e})](\partial\alpha_{2e}/\partial p_2)_T\}}$$

where γ_{2e} is the true equilibrium specific heat ratio of the dissociated diatomic gas mixture.[11, 12] A plot of both $\bar{\gamma}$ and $\hat{\gamma}_e$ vs α is given in Fig. 5. Introducing Eq. (10) and the nondimensional variables (11) into Eq. (19), one obtains, after some algebraic manipulation,

$$(\xi^2 + \eta^2)_s = \left(\frac{\beta_1 - 1}{\beta_2 - 1}\right)\frac{\hat{\gamma}_2}{\bar{\gamma}_2} \times \left\{\frac{1 - (\alpha_2 - \alpha_1)[H_D/(1+\epsilon)]}{1 + [(\bar{\gamma}_1 - 1)/(\bar{\gamma}_1 + 1)]\{[(\beta_1 - 1)/(\beta_2 - 1)](\hat{\gamma}_2/\bar{\gamma}_2) - 1\}}\right\} \qquad (20)$$

For a frozen-shock flow, Eq. (20) gives the usual result that sonic velocity occurs on a circle of radius unity in the nondimensional ξ,η hodograph plane. When the gas is in dissociation equilibrium behind the shock, a sonic locus with radii less than unity is obtained for $\alpha_2 > \alpha_1$. A typical equilibrium sonic line defined by the intersection of Eqs. (12) and (20) is shown in Fig. 3; the subsequent intersection of this line with the true equilibrium shock polar then gives the sonic point S on the polar.

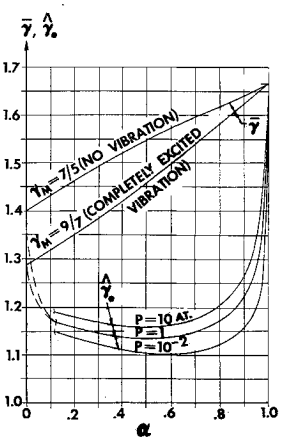

Fig. 5 Frozen and equilibrium specific heat ratios.

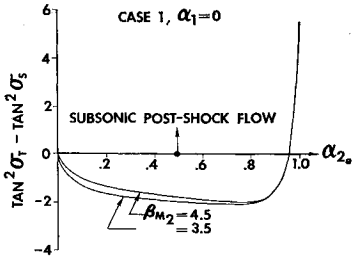

Fig. 6 Dissociation effect of position of detachment point relative to sonic point, case 1.

A useful expression for the shock angle corresponding to sonic post-shock velocity can be obtained from Eq. (20), with the aid of two general relationships derived from Eqs. (1–5). By solving Eqs. (1) and (2) for U_2 and V_2, squaring and adding the results, and converting to nondimensional form, one finds that

$$\tan^2\sigma = \frac{1 - [(\xi^2 + \eta^2)/\xi_1^2]}{[(\xi^2 + \eta^2)/\xi_1^2] - (\rho_1/\rho_2)^2} \tag{21}$$

Also, by eliminating U_2, V_2, p_2, and T_2 between Eqs. (1–5), the corresponding density ratio ρ_1/ρ_2 can be expressed in the following way[13]:

$$\frac{\rho_1}{\rho_2} = \frac{\beta_2\,[1 + (\epsilon/2\beta_1)\sin^{-2}\sigma]}{2\beta_2 - 1} - \left\{\frac{\beta_2^2[1 + (\epsilon/2\beta_1)\sin^{-2}\sigma]}{(2\beta_2 - 1)^2} - \left[\frac{1 + \epsilon\sin^{-2}\sigma - (\alpha_2 - \alpha_1)H_D}{2\beta_2 - 1}\right]\right\}^{1/2} \tag{22a}$$

$$\simeq (2\beta_2 - 1)^{-1}\left\{1 + (\beta_2 - 1)\left(1 - \left[1 + \frac{2\beta_2 - 1}{(\beta_2 - 1)^2}\times(\alpha_2 - \alpha_1)H_D\right]^{1/2}\right)\right\} \text{ for } \epsilon \to 0 \tag{22b}$$

the latter form being applicable for hypersonic flow. Thus, by using Eqs. (20) and (22), σ_s can be computed from (21) as a function of the real gas effect parameters α_2 and β_{M2}. The corresponding location of the detachment point then can be obtained and compared with σ_s by using the following relationship [Eq. (4.1.12) on p. 142 of Ref. 14]:

$$\tan^2\sigma_T = \rho_2/\rho_1 \tag{23}$$

In a perfect gas, it is well known that the detachment point occurs at slightly subsonic post-shock velocity ($\sigma_T > \sigma_s$, Fig. 4). Moreover, in the limit of hypersonic perfect gas flow, the detachment and sonic points become coincident; this is seen readily from Eqs. (20–23), where for $\epsilon = \alpha_2 = \alpha_1 = 0$, $\hat{\gamma}_2 = \bar{\gamma}_2 = \bar{\gamma}_1$, and $\beta_2 = \beta_1$, one obtains

$$[(\xi^2 + \eta^2)/\xi_1^2]_s = \rho_1/\rho_2 = (\bar{\gamma}_1 - 1)/(\bar{\gamma}_1 + 1)$$

and, hence, $\tan\sigma_s = \tan\sigma_T$. Now one can show easily that $\tan\sigma_s = \tan\sigma_T$ also holds true for hypersonic flow in a real gas when the flow across the shock is chemically frozen ($\alpha_2 = \alpha_1$, $\hat{\gamma}_2 = \bar{\gamma}_2$), regardless of the post-shock vibrational excitation (β_{M2}). However, in the case of hypersonic equilibrium shock flow involving a significant degree of post-shock dissociation relative to the freestream, a careful inspection of Eqs. (20–23) reveals that σ_T can be slightly less than σ_s. [Such a possibility has been previously observed by Hayes (Ref. 14, p. 22), although no proof was given.] That a slightly supersonic detachment point indeed does exist is confirmed readily by detailed calculation; an example is presented in Fig. 6, where $\tan^2\sigma_T - \tan^2\sigma_s$ is plotted as a function of α_{2e} and β_{M2} for the conditions pertaining to the hodograph of Fig. 3. It is seen that σ_T becomes smaller than σ_s for $\alpha_{2e} > 0$, regardless of the post-shock vibrational excitation level, except when α_{2e} is very near unity (≥ 0.95 in this example). Since the location of the detachment point on the corresponding hodograph occurs at $\alpha_{2e} \simeq 0.80$ (Fig. 3), this point clearly occurs at a slightly *supersonic* post-shock velocity. Moreover, the relative insensitivity of $\tan^2\sigma_T - \tan^2\sigma_s$ to β_{M2} and α_{2e} for $0.30 \leq \alpha_2 \leq 0.90$, shown in the present example, suggests that the detachment points for all strong equilibrium shock waves with a value of α_{2e} in this range are probably supersonic. On the other hand, it is interesting to note from Fig. 6 that, in cases where the incipiently detached shock is strong enough to produce almost complete dissociation, the usual situation of slightly subsonic post-shock velocity can be expected again.

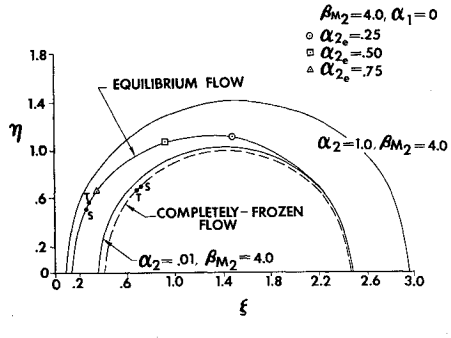

Fig. 7a Example shock polars for hypersonic flow; case 1, $\alpha_1 = 0$.

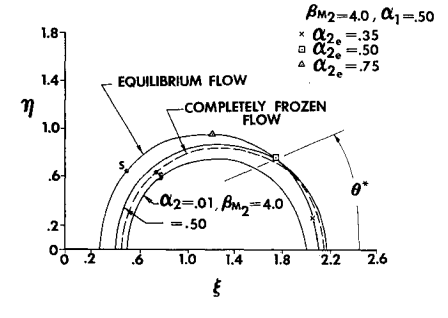

Fig. 7b Example shock polars for hypersonic flow; case 1, $\alpha_1 = 0.50$.

Real Gas Effects of the Shock Polar

Shock-polar diagrams constructed from the forementioned relations conveniently display the qualitative effects of dissociation and vibration on the velocity vector and wave geometry for all possible oblique shock solutions pertaining to a given set of freestream conditions. In the following examples, the Lighthill value of $\beta_{M2} = 4$ has been used as a reasonable average value for the entire polar, since in an actual flow β_{M2} ranges from a value of 3.5 for very weak shocks to 4.5 for the stronger shock regions on the polar. It is noted that β_{M2} was found to have a completely negligible effect on the equilibrium shock polars presented below and only a small effect on the frozen shock polars when $\alpha_2 \leq 0.50$.

Consider the example shock polars shown in Fig. 7a which pertain to a typical hypersonic flight condition in an undissociated ambient gas. Here the increasing upward departure of the shock polars for vibrationally excited and equilibrium-dissociated flow from the perfect gas shock polar clearly shows that dissociation and vibration decrease the wave angle and increase the resultant velocity behind "weak" shocks for a given flow deflection, and that they decrease the resultant velocity and increase the wave angle in the case of strong shock waves. Furthermore, it is seen that both the sonic and detachment points on the equilibrium-dissociated polar occur at a considerably larger flow deflection angle, with the sonic point lying very slightly to the left of the detachment point, as predicted in Fig. 6.

The effect of ambient gas dissociation at a given velocity can be seen by comparing Fig. 7a with the shock polars pre-

sented in Fig. 7b for $\alpha_1 = 0.50$. The polars in Fig. 7b are smaller in size because of the increased freestream specific heat ratio $\bar{\gamma}_1(\alpha_1)$ (Fig. 5). Consequently, freestream dissociation decreases the flow deflection required for detachment and the resultant velocity behind "weak" shocks, whereas it increases the velocity behind a strong shock. Furthermore, one especially can note the existence of a range of flow deflection angles $\theta \leq \theta^*$ for which the equilibrium polar lies below the polar for chemically frozen flow and $\beta_{M2} = 4$ such that $\alpha_{2e} \leq \alpha_1$.§ At $\theta = \theta^*$, the shock puts the gas into an equilibrium-dissociated state identical to that predicted by the assumption of a chemically frozen flow. The typical effect of α_1 and shock velocity on θ^* is illustrated in Figs. 8a–8c. In these hypersonic flow examples, θ^* increases very sharply with α_1 when $\alpha_1 \geq 0.25$ for a given velocity U_1. The range of shock wave angles for which $\alpha_{2e} \leq \alpha_1$ also grows rapidly as U_1 is decreased and eventually can include the entire "weak wave" branch of the shock polar. Moreover, for sufficiently small shock velocities ($\leq$ 15,000 fps), the condition $\alpha_{2e} < \alpha_1$ will occur for strong angles as well, including normal shocks as predicted from Eq. (18). Thus, a recombination-dominated exothermic relaxation to equilibrium can occur over a wide range of oblique shock angles in a highly dissociated ambient gas, in contrast to the purely endothermic dissociative relaxation that is observed behind shock waves in an undissociated ambient gas. This result is in agreement with those of several other theoretical investigations of nonequilibrium flow behind shock waves and around sharp wedges for both dissociated diatomic gases and air.[10, 13, 15, 16]

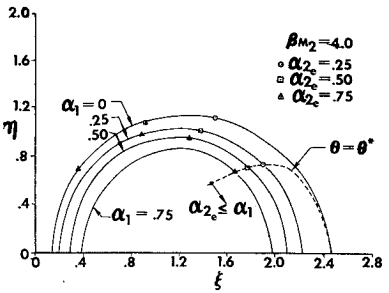

Fig. 8a Preshock dissociation effect on shock polar, case 1.

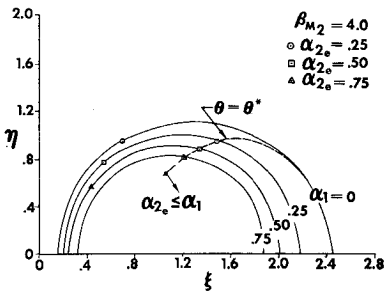

Fig. 8b Preshock dissociation effect on shock polar, case 2.

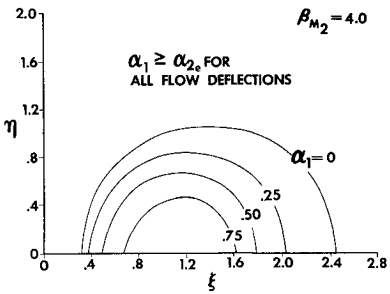

Fig. 8c Preshock dissociation effect on shock polar, case 3.

References

[1] Ferri, A., *Elements of Aerodynamics of Supersonic Flows* (The Macmillan Co., New York, 1949), pp. 49–56.

[2] Shapiro, A. H., *The Dynamics and Thermodynamics of Compressible Fluid Flow* (Ronald Press Co., New York, 1953), Vol. 1, pp. 542–544.

[3] Ames Research Staff, "Equations, tables and charts for compressible flow," NACA Rept. 1135 (1953).

[4] Feldman, S., "Hypersonic gas dynamic charts for equilibrium air," Avco Research Lab. Rept. (1957).

[5] Batchelder, R. A., "Normal and oblique shock characteristics at hypersonic speeds," Douglas Aircraft Co., Inc., Rept. LB-25599 (December 1957).

[6] Lighthill, M. J., "Dynamics of a dissociating gas; Part I, equilibrium flow," J. Fluid Mech. 2, 12 (January 1957).

[7] Liepmann, H. W. and Roshko, A., *Elements of Gasdynamics* (John Wiley and Sons, Inc., New York, 1957), pp. 29–32.

[8] Hirschfelder, J. O., "Heat transfer in chemically-reacting gas mixtures, I," J. Chem. Phys. 26, 274–281 (1957).

[9] Eschenroeder, A. Q., Boyer, D. W., and Hall, J. G., "Nonequilibrium expansions of air with coupled chemical reactions," Phys. Fluids 5, 615–624 (May 1962).

[10] Inger, G. R., "Viscous and inviscid stagnation flow in a dissociated hypervelocity free stream," *Proceedings of the 1962 Heat Transfer and Fluid Mechanics Institute* (Stanford University Press, Stanford, Calif., June 1962), pp. 95–108.

[11] Chu, B. T., "Wave propagation and the method of characteristics in reacting gas mixtures with applications to hypersonic flow," Wright Air Dev. Center TN-57-213, Armed Services Tech. Info. Agency AD-118 350 (May 1957).

[12] Inger, G. R., "One-dimensional flow of dissociated diatomic gases," Douglas Aircraft Co., Inc., Rept. SM-38523 (May 1961).

[13] Inger, G. R., "Nonequilibrium flow behind strong shock waves in a dissociated ambient gas," Douglas Aircraft Co., Inc., Rept. SM-38936 (January 1962).

[14] Hayes, W. D. and Probstein, R. F., *Hypersonic Flow Theory* (Academic Press, New York, 1959), Chap. 4, p. 142.

[15] Vincenti, W. G., "Linearized flow over a wedge in a nonequilibrium oncoming stream," Stanford Univ., Dept. Aeronaut. and Astronaut. Rept. 123 (March 1962).

[16] Capiaux, R. and Washington, M., "Nonequilibrium flow past a wedge," AIAA J. 1, 650–660 (1963).

§ Note that the completely frozen flow polar ($\alpha_2 = \alpha_1$, $\beta_{M2} = \beta_{M1}$) lies very slightly below that for chemically frozen flow in this region owing to the effect of vibration on the latter. Hence, the equilibrium and completely frozen polars intersect at a θ slightly less than θ^* where $\alpha_{2e} < \alpha_1$.